

Spin Jahn-Teller antiferromagnetism in CoTi_2O_5

Franziska K. K. Kirschner,^{1,*} Roger D. Johnson,¹ Franz Lang,¹ Dmitry D. Khalyavin,² Pascal Manuel,² Tom Lancaster,³ Dharmalingam Prabhakaran,¹ and Stephen J. Blundell^{1,†}

¹*Department of Physics, University of Oxford, Clarendon Laboratory, Parks Road, Oxford, OX1 3PU, United Kingdom*

²*ISIS Facility, Rutherford Appleton Laboratory, Harwell Oxford, Didcot OX11 0QX, United Kingdom*

³*Centre for Materials Physics, Durham University, Durham DH1 3LE, United Kingdom*

(Dated: May 23, 2022)

We have used neutron powder diffraction to solve the magnetic structure of orthorhombic CoTi_2O_5 , showing that the long-range ordered state below 26 K identified in our muon-spin rotation experiments is antiferromagnetic with propagation vector $\mathbf{k} = (\pm\frac{1}{2}, \frac{1}{2}, 0)$ and moment of $2.72(1)\mu_{\text{B}}$ per Co^{2+} ion. This long range magnetic order is incompatible with the experimentally determined crystal structure because the imposed symmetry completely frustrates the exchange coupling. We conclude that the magnetic transition must therefore be associated with a spin Jahn-Teller effect which lowers the structural symmetry and thereby relieves the frustration. These results show that CoTi_2O_5 is a highly unusual low symmetry material exhibiting a purely spin-driven lattice distortion critical to the establishment of an ordered magnetic ground state.

The Jahn-Teller effect is the spontaneous lowering of symmetry that lifts an orbital degeneracy [1] and involves a coupling of the orbital and lattice degrees of freedom. In some rather rare cases an analogous effect can occur in which spin, rather than orbital, degrees of freedom play a role. This *spin Jahn-Teller effect* has been identified in pyrochlores in which the large spin degeneracy in the lattice of corner-sharing tetrahedra can be relieved by a distortion in those tetrahedra [2, 3]. In some cubic spinels an analogous effect can take place in which a tetragonal distortion relieves the frustration [4, 5]. A related effect has also been observed near level-crossing in molecular wheels [6, 7]. In this Letter we demonstrate the existence of spin Jahn-Teller driven antiferromagnetism in CoTi_2O_5 , a compound which has much lower symmetry than either pyrochlores or spinels, showing that spin-phonon coupling can induce order in a larger class of materials than has previously been appreciated. The site symmetry of the magnetic Co^{2+} ($3d^7$) ion is $m2m$ (C_{2v}) and so the orbital levels are already non-degenerate (so no longer susceptible to a conventional Jahn-Teller transition). Nevertheless, we show that long range spin order is only permitted in the presence of the structural distortion that we predict to set in at $T_{\text{N}} = 26$ K.

Cobalt titanates are of interest due to their numerous applications. Co_2TiO_4 has a complex spinel magnetic structure [8–11], which has found uses in catalysis [12, 13], microwave devices [14], and Li-ion cells [15]. CoTiO_3 has been used as a photocatalyst [16], gas sensor [17], and also in semiconductor transistors and memory storage [18]. CoTi_2O_5 , however, is less well-studied. It is the only cobalt titanate to melt incongruently [19], and its pseudo-brookite structure [20] is an entropy-stabilized high temperature phase [21] which is susceptible to decomposition below 1414 K [22, 23]. Only recently has it become possible to synthesize high-quality single crystals of CoTi_2O_5 [24].

A polycrystalline CoTi_2O_5 powder sample was prepared using high purity ($> 99.99\%$) Co_3O_4 and TiO_2 via the solid state reaction technique. Mixed powders were sintered at 1200°C for 48h in air with intermediate grinding. After confirming the phase purity of the powder using x-ray diffraction, a cylindrical rod of diameter 10 mm and length 100 mm was sintered at 1250°C in air for 12h. Finally, the single crystal was grown in a four-mirror optical floating-zone furnace (Crystal System Inc.) in argon/oxygen mixed gas (90:10 ratio) atmosphere with a growth rate of 2–3mm/h.

Magnetic susceptibility and heat capacity data are shown in Fig. 1(a) and (b) respectively and are consistent with a magnetic transition at 26 K. The calculated entropy associated with the transition is 48% of the expected $R \ln(4)$ associated with the spin-only moment, indicative of significant correlations above T_{N} .

Zero field μSR (ZF- μSR) experiments [26, 27] were performed using a Quantum Continuous Flow Cryostat mounted on the general purpose spectrometer (GPS) at the Swiss Muon Source. All of the μSR data were analyzed using WiMDA [28].

ZF- μSR asymmetry spectra $A(t)$ are shown in Fig. 1(c). At low T , we observe an oscillatory beating pattern of $A(t)$, along with two peaks in the Fourier transform spectra [Fig. 1(d)]. This is indicative of long-range magnetic order and two inequivalent muon stopping sites. The data can be fitted either in the time domain [25] or in the field domain.

Below T_{N} , the spectral intensity $I(B)$ in the field domain can be modelled with a sum of three Lorentzian distributions:

$$I(B) = I_1 L(B; B_1, \lambda_1) + I_2 L(B; B_2, \lambda_2) + I_b L(B; 0, \lambda_b), \quad (1)$$

where $L(B; B_i, \lambda_i)$ is a Lorentzian distribution centred on B_i with a width λ_i/γ_μ ($\gamma_\mu = 2\pi \times 135.5 \text{ MHz T}^{-1}$ is

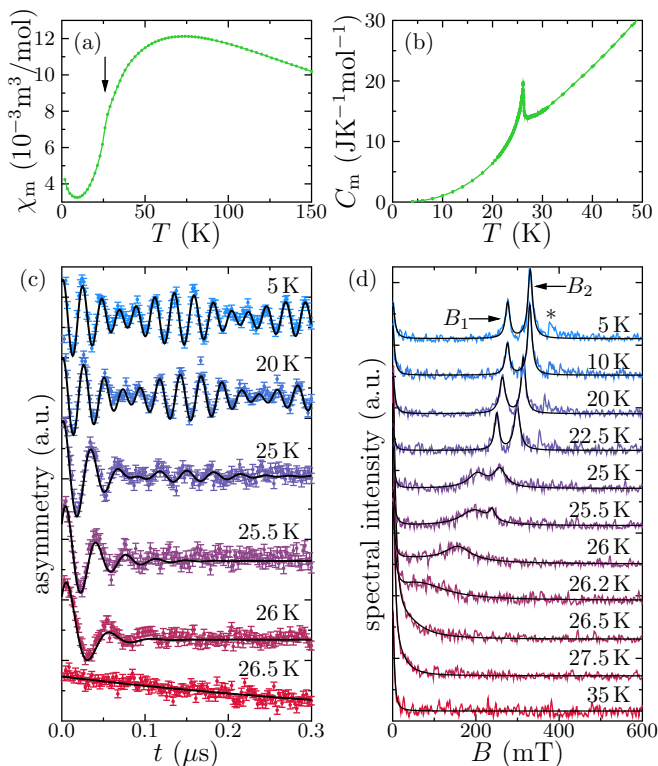


FIG. 1. (a) Magnetic susceptibility of CoTi_2O_5 measured in an applied field of $\mu_0 H = 0.1$ mT. The asterisk marks a kink at T_N . (b) Molar heat capacity. (c) ZF- μ SR spectra above and below T_N . Fits to Eq. 1 of [25] are also plotted. (d) The Fourier transform of these spectra with fits with Eq. 1. The asterisk indicates an additional feature, discussed in the main text.

the gyromagnetic ratio of the muon). The first two terms correspond to muons precessing in the internal fields of the sample; the two frequencies correspond to the two different dipolar fields at symmetry-inequivalent muon stopping sites. The Lorentzian distribution associated with each precession frequency indicates a small spread in the magnetic field distribution at the muon site, possibly due to the site disorder that has been observed between the Co and Ti sites in CoTi_2O_5 [20], small fluctuations of the Co moments, or due to muons near the boundaries of magnetic domains. The third term is a background term, corresponding to muons which land in the cryostat and sample holder, and therefore do not experience any of the sample's internal fields [the small width of this component, $\lambda_b \approx 4$ mT for all T , may be due to these muons experiencing a small field close to the surface of the sample]. The fraction of muons contributing to each peak in Fig. 1(d) f_i is given by the integral under that peak. The total fraction of muons experiencing a non-zero field, $f_B = (f_1 + f_2) / (f_1 + f_2 + f_3)$, is plotted in Fig. 2(a). The drop in f_B above T_N marks the transition into the paramagnetic state.

The fitted values from Eq. 1 for the T evolution of

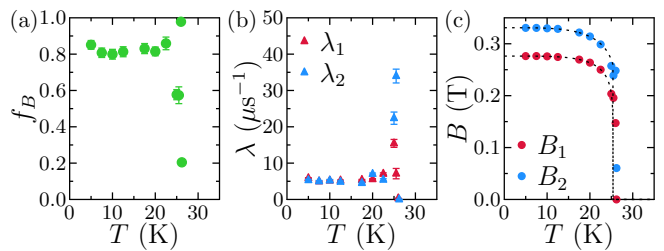


FIG. 2. (a) Temperature dependence of the fraction of muons experiencing a coherent magnetic field. Temperature dependences of the peak width and centers, as fitted from Eq. 1 applied to the Fourier transform of the ZF- μ SR spectra, are shown in (b) and (c) respectively. The dotted lines in (c) show phenomenological fits [25].

λ_i and B_i are presented in Figs. 2(b) and (c) respectively. As T increases towards T_N , the two peaks broaden and merge, while their centers move towards 0 T as the long-range-ordered magnet transitions to the paramagnetic regime. The data in Fig. 2(c) were fitted with the phenomenological formula $B = B_0 (1 - (T/T_N)^\alpha)^\beta$ [25], giving $T_N = 26.0(11)$ K for both components. We also find values of the internal fields at the muon sites as $T \rightarrow 0$: $B_1 = 330(3)$ mT and $B_2 = 276(6)$ mT. There appears to be an additional small feature in the data at low T at ≈ 400 mT (marked by the asterisk in Fig. 1(d)), which may arise due to the site disorder and is discussed below.

Neutron powder diffraction (NPD) measurements were performed on the WISH time-of-flight diffractometer [29] at ISIS, the UK Neutron and Muon Source. A highly pure, single crystal sample was ground to a fine powder and loaded into a cylindrical vanadium can, which was mounted within a ^4He cryostat. Data were collected with high counting statistics at 1.5 K, deep into the long-range ordered magnetic phase, and at 100 K in the paramagnetic phase. All diffraction data were refined using FULLPROF [30].

NPD data collected at 100 K (well above any anomalies in χ) were fitted with a nuclear model based upon the published crystal structure [20]. The goodness-of-fit was excellent, the data and fit are shown in Fig. 3(a), and the refined structural parameters are given in [25]. There was no evidence of impurity phases in these data. There is a small amount of site mixing whereby 2.8% of Co sites are occupied by Ti, and 1.4% of Ti sites are occupied by Co.

When compared to the NPD pattern at 100 K, data collected at 1.5 K showed more than 10 new diffraction peaks (Fig. 3(b)). Based on bulk properties measurements [25] and the results of our ZF- μ SR experiments, we could robustly assign the origin of the new intensities to long-range magnetic order. The observation of such a large number of magnetic diffraction peaks allowed us to unambiguously determine the magnetic propaga-

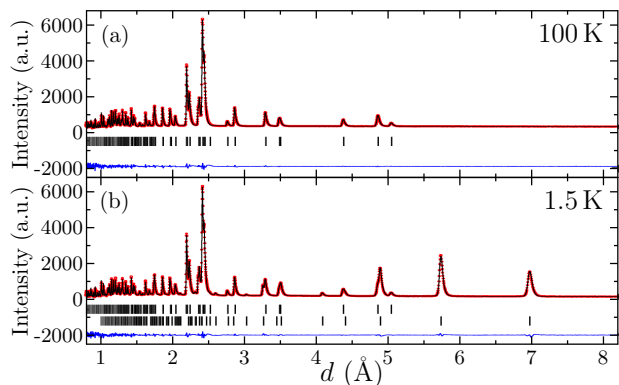


FIG. 3. Neutron powder diffraction data (red points) measured in bank 2 (average $2\theta = 58.3^\circ$) of the WISH diffractometer from CoTi_2O_5 in (a) the paramagnetic phase and (b) the antiferromagnetic phase. The fitted $Cmcm$ nuclear model (a) and nuclear + magnetic model (b), as described in the text, are shown as solid black lines. The respective peak positions are shown as black tick marks (nuclear top, magnetic bottom). Difference patterns ($I_{\text{obs}} - I_{\text{calc}}$) are given as solid blue lines at the bottom of the panes.

tion vector, which was found to be $\mathbf{k}_1 = (\frac{1}{2}, \frac{1}{2}, 0)$, or $\mathbf{k}_2 = (-\frac{1}{2}, \frac{1}{2}, 0)$, or both. Note that these two vectors are distinct, i.e. they are not related by an allowed reciprocal lattice vector of the C-centred parent structure, yet they cannot be differentiated by powder diffraction.

Symmetry analysis was performed using the ISOTROPY Suite [4,5], taking the $Cmcm$ crystal structure of CoTi_2O_5 [20] as the parent. Four irreducible representations enter into the decomposition of the magnetic reducible representation of \mathbf{k}_1 and \mathbf{k}_2 for the relevant Co Wyckoff positions. Through systematic tests it was found that the magnetic structures of just one irreducible representation, mS_2^- , reproduced the relative intensities of the magnetic diffraction peaks. In this discussion, we make reference to four symmetry-equivalent crystallographic sites, defined with respect to the $Cmcm$ unit cell, which comprise the full cobalt sublattice: Co1: $[0, y, \frac{1}{4}]$; Co2: $[\frac{1}{2}, \frac{1}{2} - y, \frac{3}{4}]$; Co3: $[\frac{1}{2}, \frac{1}{2} + y, \frac{1}{4}]$; Co4: $[0, 1 - y, \frac{3}{4}]$, where $y = 0.1911(6)$ at 100 K.

Matrices of the two dimensional irreducible representation mS_2^- , for selected symmetry generators of the parent space group $Cmcm$, are given in the top row of Table S.II [25]. The magnetic order parameter can take one of three distinct directions in the space spanned by the irreducible representation: (η, η) , $(\eta, 0)$, or (η, ϵ) . In all cases, the respective magnetic structures involve moments oriented strictly parallel to the orthorhombic c axis. As all of the Co ions in the lattice are structurally equivalent, and therefore have the same chemical environment, all of the moments on these ions are constrained to be equal in magnitude. The only order parameter direction consistent with this constraint is $(\eta, 0)$.

$(\eta, 0)$ corresponds to a magnetic structure that low-

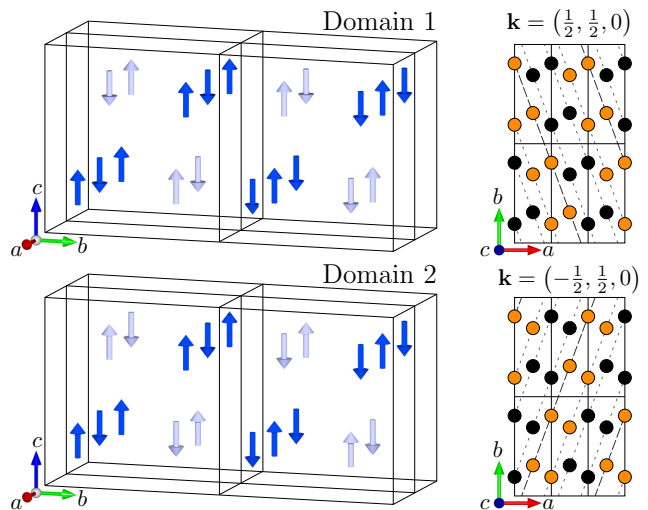


FIG. 4. The magnetic structure of CoTi_2O_5 . In the left hand panes four $Cmcm$ unit cells are drawn, which represent a full repeating unit of the magnetic structure. Co1 and Co4 moments, drawn as dark blue arrows, are related to the Co2 and Co3 moments, drawn as light blue arrows, by C-centring. Note that the two domains related by the $\{m_x|0, 0, 0\}$ symmetry operator of the parent structure can be obtained by reversing the sign of the Co2 and Co3 moments. The diagrams on the right hand side illustrate the two propagation vectors associated with the two domains, where antiparallel moments are drawn as orange and black spheres. Planes of parallel moments are denoted by faint dotted grey lines, and the periodicity of the magnetic structure is highlighted by the bold dashed grey lines.

ers the symmetry of the system to monoclinic (magnetic space group P_a2_1/m [31]). Magnetic moments on the Co1, Co2 and Co4 sites are parallel, but with the moment on the Co3 sites aligned antiparallel. A second domain exists with order parameter $(0, \eta)$, in which Co1, Co3, and Co4 sites are aligned parallel to each other, with Co2 antiparallel. Inspection of the mS_2^- matrices given in Table S.II [25] shows that the $(\eta, 0)$ and $(0, \eta)$ magnetic domains are interchanged by the symmetry operator $\{m_x|0, 0, 0\}$, which is indeed broken below the magnetic phase transition. Furthermore, the $(\eta, 0)$ and $(0, \eta)$ domains are described by single propagation vectors, \mathbf{k}_1 and \mathbf{k}_2 , respectively, which are also related by m_x . The two domains are shown in Fig. 4, with the schematic in the right hand panes illustrating the two propagation vector directions. We note that the two domains are indistinguishable in our powder diffraction data. The magnitude of the Co moment was refined against the diffraction data and found to be $2.72(1) \mu_B$ at 1.5 K (see Fig. 3(b)).

The only nearest neighbour, super-exchange interactions between cobalt atoms (Co–O–Co) connect magnetic moments along the a -axis in $\text{Co}_i\text{--Co}_i$ chains. All other nearest-neighbour interactions are mediated by super-super-exchange (Co–O–O–Co). One can assume that the super-exchange interactions are dominant and, by the

experimentally determined magnetic structure, are antiferromagnetic. All exchange interactions between the (Co1,Co4) and (Co2,Co3) sites, coloured dark and light blue in Fig. 4 respectively, are exactly frustrated by the m_x symmetry element. This frustration will likely lead to one dimensional ordering of the a -axis chains above T_N , but below the mean field energy of the dominant super-exchange interaction, consistent with the missing entropy evidenced in the heat capacity. For long range order to develop in CoTi_2O_5 , the m_x mirror symmetry must be broken either at a structural phase transition above T_N , or through the spin Jahn-Teller effect, in which the primary magnetic order parameter couples to a secondary, symmetry breaking structural order parameter spontaneously at T_N [2, 3]. In the absence of any experimental evidence for a higher T structural phase transition, we discuss possible magneto-structural coupling schemes.

The lowest order, free energy invariant that can couple the magnetic order to symmetry breaking crystallographic distortions must be quadratic in the magnetic moments (to be time-reversal even), and linear in the structural order parameter. On traversing the crystal in the direction of the propagation vector, magnetic moments change sign from one unit cell to the next. However, in the square of the moments each unit cell is the same. Hence, the square of the order parameter components, η^2 and ϵ^2 , must couple to a $\mathbf{k}_s = (0, 0, 0)$, Γ -point structural distortion if the coupling term is to be invariant by translation, as required. Through exhaustive searches performed using the ISOTROPY suite [32, 33], the only linear-quadratic invariant that can couple a non-trivial Γ -point structural distortion to the magnetic order is $\delta(\eta^2 - \epsilon^2)$, where the irreducible representation of the structural order parameter, δ , is Γ_2^+ . For completeness, we should also consider the trivial coupling invariant $\xi(\eta^2 + \epsilon^2)$, where the structural order parameter ξ transforms according to the totally symmetric Γ_1^+ irreducible representation, i.e. structural distortions that were already allowed within the $Cmcm$ parent symmetry can also occur at T_N . The atomic displacements of Γ_1^+ and Γ_2^+ are tabulated in [25]. High resolution laboratory based x-ray powder diffraction experiments yielded no evidence of these distortions below T_N . We therefore assume that any structural distortion in CoTi_2O_5 will be small, and the following calculations utilize the undistorted unit cell.

In order to establish the potential muon stopping sites in CoTi_2O_5 , we employed Density Functional Theory (DFT) calculations to map out the electrostatic Coulomb potential of CoTi_2O_5 throughout its unit cell [25], plotted using the VESTA software [34] in Fig 5(a). The maxima of such a potential map are a reliable approximation to the muon sites as they correspond to low energies needed to add a positive charge, such as the muon [35, 36]. We also carried out relaxation calculations [25],

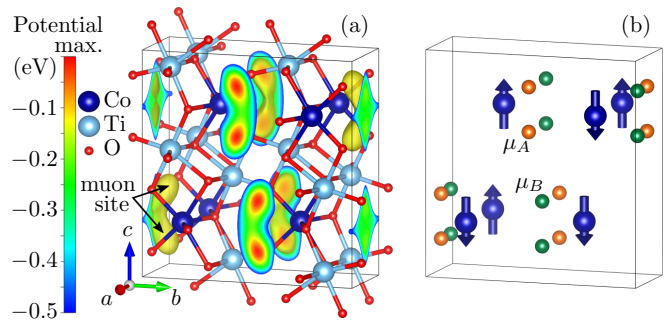


FIG. 5. (a) Electrostatic Coulomb potential of CoTi_2O_5 computed with DFT. The potential is shown on the surface of the unit cell up to 0.5 eV below its maximum value, and a yellow isosurface is plotted within the unit cell at 0.25 eV below the maximum. (b) Muon positions inside CoTi_2O_5 , with the two symmetry inequivalent groups μ_A and μ_B marked in orange and green respectively. The spin structure of domain 1 is shown on the Co ions.

which allow for local distortions of the lattice caused by the muon's presence. These gave a single symmetry-inequivalent muon stopping site at the general position $[0.322, 0.03, 0.151]$ with a 1.0 \AA O-H-like bond with the nearest oxygen. This is in line with the approximate position we identified from the electrostatic potential.

There are 16 symmetry equivalent muon sites in the $Cmcm$ parent structure, which are split into two groups of eight in the magnetic unit cell, related by the broken m_x symmetry, and are denoted by μ_A and μ_B in Fig. 5(b). The muon stopping probability is dependent upon the electrostatic potential local to the stopping sites, and under a small structural distortion induced at the phase transition, μ_A and μ_B become structurally inequivalent, and are therefore associated with different muon stopping probabilities. Changing from one magnetoelastic domain to another swaps the stopping probabilities of the two subgroups [25]. The symmetry of the magnetic structure also dictates that μ_A and μ_B will have different local magnetic fields: we calculate these to be $335(1) \text{ mT}$ and $277(1) \text{ mT}$, in excellent agreement with our experimental observations at low T . As the area under the higher-field peak in Fig. 1(d) is larger than that of the lower-field peak, this suggests that the muon site experiencing this field is preferentially occupied. By comparing the energies at the muon sites under small distortions, we present a possible coupling between a shear distortion and the magnetic domains in [25] that could explain this.

Finally we consider the additional feature marked by an asterisk in Fig. 1(d) at $\approx 400 \text{ mT}$. This feature likely arises due to a Co ion occupying the nearest Ti site so that a small fraction of muons stopping close to this defect experience a slightly larger field. Indeed, modelling this disorder gives a field at the muon site of $\approx 410 \text{ mT}$, consistent with the experimental value.

To conclude, we have identified long range magnetic order in CoTi_2O_5 , which is antiferromagnetic with $\mathbf{k} = (\pm\frac{1}{2}, \frac{1}{2}, 0)$. Frustration in the super-super-exchange interactions, along with the absence of a structural distortion above $T_N \approx 26\text{ K}$, indicate that the magnetic transition must be coupled to a structural transition at T_N in order to relieve the frustration. This coupling occurs due to the spin Jahn-Teller effect, which has so far only been identified in higher-symmetry crystal structures [2–5]. Our results show that magnetic order driven by spin-phonon coupling can be extended to lower-symmetry systems. While the predicted distortion in CoTi_2O_5 was not resolvable in high resolution laboratory based x-ray powder diffraction experiments, it may be possible to resolve using higher-resolution synchrotron x-ray powder diffraction experiments. The study of compounds structurally related to CoTi_2O_5 may provide further insight into the conditions required for the spin Jahn-Teller effect to, or not to, occur.

Acknowledgements. F.K.K.K. thanks Lincoln College, Oxford, for a doctoral studentship. R.D.J. acknowledges support from a Royal Society University Research Fellowship. This work is supported by EPSRC (UK) grant EP/N023803/1. Part of this work was performed at the Science and Technology Facilities Council (STFC) ISIS Facility, Rutherford Appleton Laboratory, and part at μS , the Swiss Muon Source (PSI, Switzerland). The authors would like to acknowledge the use of the University of Oxford Advanced Research Computing (ARC) facility in carrying out this work [37].

* franziska.kirschner@physics.ox.ac.uk

† stephen.blundell@physics.ox.ac.uk

- [1] G. A. Gehring and K. A. Gehring, *Rep. Prog. Phys.* **38**, 1 (1975).
- [2] Y. Yamashita and K. Ueda, *Phys. Rev. Lett.* **85**, 4960 (2000).
- [3] O. Tchernyshyov, R. Moessner, and S. L. Sondhi, *Phys. Rev. Lett.* **88**, 067203 (2002).
- [4] M. Onoda and J. Hasegawa, *J. Phys. Condens. Matter* **15**, L95 (2003).
- [5] T. Watanabe, S. I. Ishikawa, H. Suzuki, Y. Kousaka, and K. Tomiyasu, *Phys. Rev. B* **86**, 144413 (2012).
- [6] O. Waldmann, C. Dobe, S. T. Ochsenbein, H. U. Güdel, and I. Sheikin, *Phys. Rev. Lett.* **96**, 027206 (2006).
- [7] O. Waldmann, *Phys. Rev. B* **75**, 174440 (2007).
- [8] S. Ogawa and S. Waki, *J. Phys. Soc. Jpn.* **20**, 540 (1965).
- [9] J. K. Srivastava, S. Ramakrishnan, V. R. Marathe, G. Chandra, R. Vijayaraghava, J. A. Kulkarni, V. S. Darshane, and S. Singh, *J. Phys. C* **20**, 2139 (1987).
- [10] G. Gavoiile, J. Hubsch, and S. Koutani, *J. Magn. Magn. Mater.* **102**, 283 (1991).
- [11] S. Nayak, S. Thota, D. C. Joshi, M. Krautz, A. Waske, A. Behler, J. Eckert, T. Sarkar, M. S. Andersson, R. Mathieu, V. Narang, and M. S. Seehra, *Phys. Rev. B* **92**, 214434 (2015).
- [12] D.-C. Kim and S.-K. Ihm, *Environ. Sci. Technol.* **35**, 222 (2001).
- [13] J. Zhu and Q. Gao, *Microporous and Mesoporous Mater.* **124**, 144 (2009).
- [14] V. G. Harris, A. Geiler, Y. Chen, S. D. Yoon, M. Wu, A. Yang, Z. Chen, P. He, P. V. Parimi, X. Zuo, C. E. Patton, M. Abe, O. Acher, and C. Vittoria, *J. Magn. Magn. Mater.* **321**, 2035 (2009).
- [15] C. P. Sandhya, B. John, and C. Gouri, *Ionics* **20**, 601 (2014).
- [16] R. Ye, H. Fang, Y.-Z. Zheng, N. Li, Y. Wang, and X. Tao, *ACS Appl. Mater. Interfaces* **8**, 13879 (2016).
- [17] X. Chu, X. Liu, G. Wang, and G. Meng, *Mater. Res. Bull.* **34**, 1789 (1999).
- [18] T. S. Chao, W. M. Ku, H. C. Lin, D. Landheer, Y. Y. Wang, and Y. Mori, *IEEE Trans. Electron Devices* **51**, 2200 (2004).
- [19] B. Brezny and A. Muan, *J. Inorg. Nucl. Chem.* **31**, 649 (1969).
- [20] H. Müller-Buschbaum and M. Waburg, *Monatsh Chem.* **114**, 21 (1983).
- [21] A. Navrotsky, *Am. Mineral.* **60**, 249 (1975).
- [22] A. Yankin, O. Vikhreva, and V. Balakirev, *J. Phys. Chem. Solids* **60**, 139 (1999).
- [23] K. T. Jacob and G. Rajitha, *J. Chem. Thermodyn.* **42**, 879 (2010).
- [24] A. M. Balbashov, A. A. Mukhin, V. Y. Ivanov, L. D. Iskhakova, and M. E. Voronchikhina, *Low Temp. Phys* **43**, 965 (2017).
- [25] See Supplemental Material at [URL will be inserted by publisher] for further data fitting and measured parameters, details of the DFT calculations, and a discussion of structural order parameters and lattice distortions.
- [26] S. J. Blundell, *Contemp. Phys.* **40**, 175 (1999).
- [27] A. A. Yaouanc and P. D. de Réotier, *Muon spin rotation, relaxation, and resonance : applications to condensed matter* (Oxford University Press, 2011) p. 486.
- [28] F. L. Pratt, *Physica B* **710**, 289 (2000).
- [29] L. C. Chapon, P. Manuel, P. G. Radaelli, C. Benson, L. Perrott, S. Ansell, N. J. Rhodes, D. Raspino, D. Duxbury, E. Spill, and J. Norris, *Neutron News* **22**, 22 (2011).
- [30] J. Rodríguez-Carvajal, *Physica B* **192**, 55 (1993).
- [31] The P_a2_1/m magnetic unit cell has a $\{[-2, 0, 0], [0, 0, 1], [\frac{1}{2}, \frac{1}{2}, 0]\}$ change of basis with respect to the $Cmcm$ parent structure, plus an origin shift of $[-\frac{1}{4}, \frac{1}{4}, 0]$. N.B. The orthorhombic $Cmcm$ c -axis is parallel to the P_a2_1/m b -axis in the standard setting.
- [32] B. J. Campbell, H. T. Stokes, D. E. Tanner, and D. M. Hatch, *J. Appl. Crystallogr.* **39**, 607 (2006).
- [33] H. T. Stokes, D. M. Hatch, and B. J. Campbell, *ISOTROPY Software Suite* (2007).
- [34] K. Momma and F. Izumi, *J. Appl. Crystallogr.* **41**, 653 (2008).
- [35] J. S. Möller, P. Bonfà, D. Ceresoli, F. Bernardini, S. J. Blundell, T. Lancaster, R. De Renzi, N. Marzari, I. Watanabe, S. Sulaiman, and M. I. Mohamed-Ibrahim, *Phys. Scripta* **6**, 068510 (2013).
- [36] F. R. Foronda, F. Lang, J. S. Möller, T. Lancaster, A. T. Boothroyd, F. L. Pratt, S. R. Giblin, D. Prabhakaran, and S. J. Blundell, *Phys. Rev. Lett.* **114**, 017602 (2015).
- [37] A. Richards, <https://doi.org/10.5281/zenodo.22558> (2015).